Micellar TIA1 with folded RNA binding domains as a model for reversible stress granule formation

Keith J. Fritzsching[a], Yizhuo Yang[a], Emily M. Pogue[a], Joseph B. Rayman[b,c], Eric R. Kandel[b,c,d,e,f], and Ann E. McDermott[a,1]

[a]Department of Chemistry, Columbia University, New York, NY 10027; [b]Department of Neuroscience, College of Physicians and Surgeons, Columbia University, New York, NY 10032; [c]Department of Psychiatry, College of Physicians and Surgeons, Columbia University, New York, NY 10032; [d]HHMI, Columbia University, New York, NY 10032; [e]Zuckerman Mind Brain Behavior Institute, Columbia University, New York, NY 10032; and [f]Kavli Institute for Brain Science, Columbia University, New York, NY 10032

Contributed by Ann E. McDermott, September 24, 2020 (sent for review April 20, 2020; reviewed by Bernd Reif and Robert Tycko)

TIA1, a protein critical for eukaryotic stress response and stress granule formation, is structurally characterized in full-length form. TIA1 contains three RNA recognition motifs (RRMs) and a C-terminal low-complexity domain, sometimes referred to as a "prion-related domain" or associated with amyloid formation. Under mild conditions, full-length (fl) mouse TIA1 spontaneously oligomerizes to form a metastable colloid-like suspension. RRM2 and RRM3, known to be critical for function, are folded similarly in excised domains and this oligomeric form of apo fl TIA1, based on NMR chemical shifts. By contrast, the termini were not detected by NMR and are unlikely to be amyloid-like. We were able to assign the NMR shifts with the aid of previously assigned solution-state shifts for the RRM2,3 isolated domains and homology modeling. We present a micellar model of fl TIA1 wherein RRM2 and RRM3 are colocalized, ordered, hydrated, and available for nucleotide binding. At the same time, the termini are disordered and phase separated, reminiscent of stress granule substructure or nanoscale liquid droplets.

solid-state NMR | stress granule | RNA binding protein | membranelles organelles | prion

T cell intracellular antigen-1 (TIA1) has multiple roles within cells, including a critical role in stress granule (SG) formation during eukaryotic cellular stress response (1–3) and translation regulation (4–6). SGs appear in cells exposed to stressors, such as pH, oxidation, and temperature changes, and contain stalled preinitiation RNA–protein complexes. They have been hypothesized to act as a decision point in mRNA processing by helping to guide homeostasis-restoring protein expression or begin apoptosis. Although sometimes associated with misfolded protein aggregates, SG components dissolve and regain function more quickly than other aggregates after the stress is removed (7). TIA1 has three RNA recognition motifs (RRM1, RRM2, RRM3) known to bind RNA with relatively little sequence specificity. TIA1 has a C-terminal low-complexity domain (LCD) enriched with asparagine and glutamine that has been referred to in the literature as a prion-related domain (PRD) because of its sequence similarity to amyloid- or prion-forming proteins. Proteins associated with SGs have also been linked to several human diseases, some characterized as protein misfolding disorders. A mutation within the LCD of TIA1 is the diagnostic marker for Welander distal myopathy (8, 9), and several other TIA1 mutations are linked to amyotrophic lateral sclerosis (10).

Despite its importance, little is known about the full-length (fl) or oligomeric form(s) of TIA1 or about the LCD. The RRM domains have been structurally characterized (11–13), giving insight into structure, dynamics, binding, and function. Several excised TIA1-RRM domain constructs were characterized with small-angle scattering and liquid-state NMR; the LCD was excluded from the constructs used in prior published structural studies (11, 13). NMR was used to solve the structure of TIA1-RRM1 (Protein Data Bank [PDB] ID code 5O2V), TIA1-RRM2 bound to the dinucleotide UU-RNA (PDB ID code 5O3J), and TIA1-RRM2,3 (PDB ID code 2MJN). RRM1 appears to contribute little to RNA binding, which may be explained by the negatively charged residues in the RNP1 motif within RRM1. A model of rigid RRM domains with flexible linkers was used to interpret scattering data and show that RRM2 and RRM3 associate more closely with each other and more so after RNA binding than with RRM1. However, the effects of the LCD on the fl structure have remained elusive due to experimental challenges.

It has been reported that the LCD of TIA1 can cause phase separation (14). In vivo, phase separation of groups of functionally related, locally concentrated proteins and nucleic acids (14) is believed to lead to the formation of membraneless organelles (biomolecular condensates), such as stress granules (15). Many cellular condensates contain proteins with RNA-binding domains, including Cajal bodies, P bodies, and SGs (15). Misregulation of phase separation has been implicated in several human disease-related functions (8, 9).

Many proteins with LCDs also spontaneously partition into separate phases or form gels at high concentrations in vitro, potentially providing a model for in vivo phase separation. The in vitro systems share important properties with the corresponding in vivo systems. Both can undergo transitions and display a continuum of mechanical properties from liquid-like droplets to glassy (16), solid-like particles. Liquid–liquid droplets are typically micrometer, morphologically spherical domains that exhibit liquid-like dynamics in their rapid recovery from photobleaching and solution-state NMR spectra (17). Many liquid droplets or condensates in vitro are metastable and transform over time (16, 18) in a process referred to as hardening or

Significance

Structural characterization of fl mouse TIA1 (43 kDa monomer) with solid-state NMR reveals structured functional domains and a disordered low-complexity domain. These data are consistent with a micellar form of apo fl TIA, unexpected based on much previous literature. We expect that these models of TIA1 and the NMR approaches will help us understand many similar proteins and their roles in the cellular stress response.

Author contributions: K.J.F. and A.E.M. designed research; K.J.F., Y.Y., and E.M.P. performed research; J.B.R. contributed new reagents/analytic tools; K.J.F., Y.Y., and A.E.M. analyzed data; K.J.F., E.M.P., J.B.R., E.R.K., and A.E.M. wrote the paper; and E.R.K. and A.E.M. supervised.

Reviewers: B.R., Technical University Munich; and R.T., National Institute of Diabetes and Digestive and Kidney Diseases.

The authors declare no competing interest.

[1]To whom correspondence may be addressed. Email: aem5@columbia.edu.

This article contains supporting information online at https://www.pnas.org/lookup/suppl/doi:10.1073/pnas.2007423117/-/DCSupplemental.

First published November 30, 2020.

maturation (7, 10, 16, 19). Analogously, membraneless organelles can undergo transitions in vivo during regulated maturation processes (15, 20, 21). Thus, it has been suggested that misfolded, amyloid-like fibrils and aggregates form during maturation of the membraneless organelles (7), suggesting a role for condensates in templating the formation of disease-related fibrils (22). Furthermore, the multiphase in vitro suspensions can be compared to colloids, in that they are homogeneously distributed, stable multiphase suspensions whose formation is controlled by salt concentration, viscogens, and temperature. However useful these analogies are, it is important to note that the in vitro systems are, of course, highly simplified compared to the in vivo situation. The in vivo systems are subject to important biological control over their formation and dissolution and include many other components such as nucleic acids and other proteins.

The LCD/PRD of TIA1 has primary sequence similarity to the better-characterized SUP35 prion protein and is also similar to other amyloid-forming proteins (23–25). Atomic force and electron microscopy (EM) have been used to show that TIA1 forms fibers under some conditions (26, 27). Congo red and thioflavin T binding assays have been used to suggest TIA1 forms a cross-β amyloid (26, 28). Sup35 and FUS are proteins with a domain structure and an LCD analogous to TIA1; both have been reported to form amyloids (29). Alternatively, it has been hypothesized that the LCD in multidomain proteins can be unfolded (intrinsically disordered) even in the functional form and that oligomerization might be driven by nonspecific intermolecular interactions between several LCDs on different monomers (7, 30, 31). A dominant hypothesis in the literature has been that the LCD induces disease-related amyloid formation. Many proposed functions of TIA1, such as RNA sequestration into SGs (16), raise the question of whether the RRM domains are folded in the condensates or high-order oligomeric forms.

Here we report structural studies of fl apo TIA1 prepared without the use of harsh solvents or denaturants. High-order oligomeric systems such as amyloid fibrils are often challenging systems for traditional structural biology methods. However, solid-state NMR (SSNMR) and EM have been powerful tools for studying these systems. We characterize fl TIA1 with EM and SSNMR to test for the presence of a solid-like phase (fibril), a liquid-like phase (intrinsically disordered protein), or some other structure. We address which domains are folded or ordered, which are solvent exposed, and whether the oligomeric structure is compatible with binding at the RRMs. The answers to these intensely debated questions have consequences for future studies of biomolecular condensates.

Methods

To avoid expression into inclusion bodies and the need for denaturants during purification, we added a tobacco etch virus protease (TEV) cleavable His6-SUMO solubility tag to the C terminus. After immobilized metal affinity chromatography purification, the solubility tag was cleaved. Final purification of TIA1 was done in high ionic strength buffers to limit oligomerization.

The suspension oligomerized TIA in the NMR buffer was pelleted and packed into 3.2 mm Bruker-style rotors by centrifugation. NMR experiments were conducted on a 900 MHz Bruker Avance II, a 750 MHz Bruker Avance I, or a 750 MHz Bruker NEO spectrometer. At each field, a 3.2 mm Bruker Efree HCN probe was used. The set temperature was 258 ± 5 K, and the magic-angle spinning frequency was 16.666 kHz. A full description of the methods is in *SI Appendix*.

Results

We recombinantly expressed and purified fl *Mus musculus* (mouse) TIA1 (*SI Appendix*, Scheme S1) in high yield (>20 mg/L) using mild conditions as described in *Methods*. Concentrated solutions of TIA1 (>0.5 mg/mL) at pH 6.8 and near physiological ionic strength (50 to 300 mM sodium chloride) tended to separate into a protein-rich phase and an aqueous phase without substantial protein over a few hours. The TIA1-enriched phase scattered light and was denser than the surrounding solution, as shown in Fig. 1*C*. The separation (monitored by scattering) was accelerated by stirring or agitation. The protein-enriched phase could be sedimented with excellent yield using gentle centrifugation (gravity overnight with no agitation or with moderate centrifugation as described in *Methods*); no residual soluble TIA1 in the supernatant was detected by ultraviolet-visible spectroscopy. The phase separation is reversible; dilution and gentle agitation or an increase in ionic strength rehomogenize the solution. The fact that the protein sediments at low *g* force suggests that under these mild aqueous conditions, the fl protein forms a high-order oligomer. The dense protein phase following centrifugation is reminiscent of a metastable colloid-like suspension. It forms reversibly in a manner dependent on cosolutes, appears to have dispersed particles, and is stable for many hours. We think of the TIA1 samples prepared in this way as colloidal homo-oligomeric apo (absence of RNA) wild-type full-length mouse TIA1 and refer to this kind of preparation whenever discussing fl TIA1 (unless otherwise specified). While the properties in many ways resembled colloids, they were a poor match for amyloid fibrils or disordered precipitates, as elaborated below.

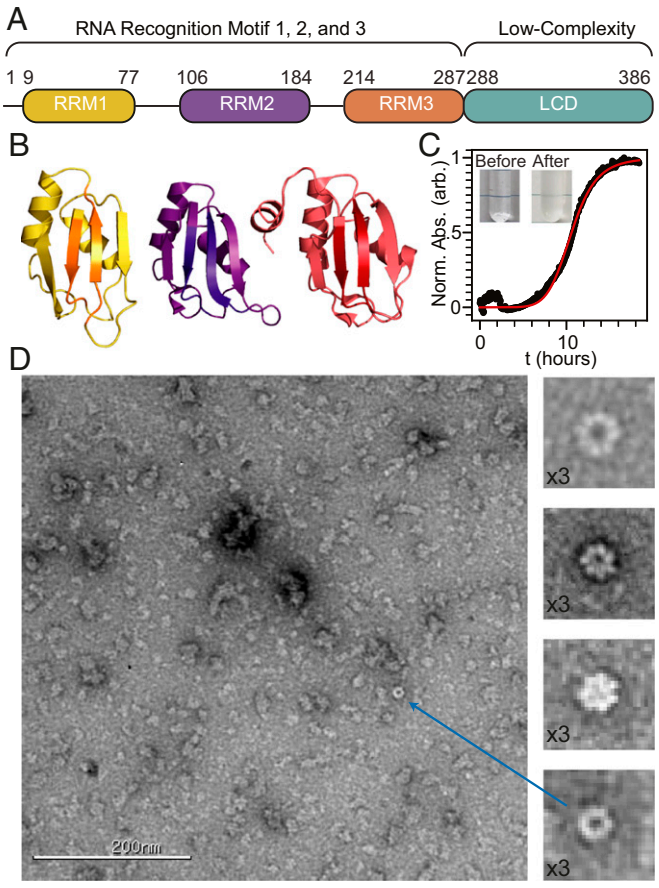

Fig. 1. (*A*) Domain structure of TIA1. (*B*) RRM1 (yellow), RRM2 (purple), and RRM3 (red) homology models are based on PDB ID code 2CQI and PDB ID code 2MJN. (*C*) Scattering (normalized absorbance) of 550 nm light by an ~2 mg/mL fl TIA1 solution. The solution became opaque after 5 to 10 h. The data were fit (red) with the Hill equation with a Hill coefficient of 7. Images taken before and after show an increase in opacity. (*D*) Negatively stained electron micrographs of TIA1. Fibrils were not observed. Instead, we observed irregular oligomers. In some micrographs, disklike or spherical particles with clear, oligomeric substructures were observed, such as in the inset expansions. (Magnification: 3×.)

Negatively stained transmission EM of fl TIA1 did not show fibrils. Our stained EM images consistently gave evidence of nanometer-scale, irregular protein deposits, consistent with the proposal that the protein is present in oligomeric form (Fig. 1*D*). A relatively small fraction of observed particles presented with a circular (spherical or disk) morphology, suggestive of oligomers with at least six to eight copies visible in the focal plane.

The high-field, multidimensional SSNMR spectra of fl TIA1 show segments that are exceptionally well ordered on an atomic scale. There are many resolved peaks with narrow linewidths in cross-polarization (CP) based ^{13}C–^{13}C correlation spectra of U–^{13}C,^{15}N TIA1 (Fig. 2 *A*–*F*). The ^{13}C NMR peaks show dispersion within typical amino acid chemical shift ranges (32), indicating the presence of mixed secondary structures, including helix and sheet. The spectra show no substantial batch-to-batch variation (*SI Appendix*, Fig. S3), peak doubling, or other spectral indications of polymorphism and were stable for weeks under experimental conditions. Together, these data indicate that some segments of TIA1 are homogeneous and well ordered in the oligomers.

We counted the resolved peaks within the characteristic chemical shift ranges of several amino acids to estimate the number of specific amino acids that are ordered or folded. In the two-dimensional (2D) ^{13}C–^{13}C spectra the following are partially or fully resolved: 11 Ala, 11 Gly, 10 Pro, 11 Thr, 11 Ser, 11 Val, and 12 Phe. Phe peaks were resolved in a sample labeled with only ^{13}C,^{15}N Phe and ^{15}N Val (see *SI Appendix*, Fig. S4). Ala peaks were additionally resolved in a sample labeled with only ^{13}C Ala, ^{15}N Gly, and ^{15}N Tyr (see *SI Appendix*, Fig. S5).These selectively labeled samples corroborated the finding from the uniform sample in all cases. Assuming that these observed peaks arise from a contiguous segment of the primary sequence, the minimum length subsequence that can explain these residues spans approximately residues 110 to 298, including RRM2 and RRM3 but not RRM1 or the LCD (Fig. 2*G*). We hypothesize, therefore, that a contiguous segment including RRM2,3 is folded and ordered in fl TIA1. AG and AY amino acid pairs are found in only TIA1 in the RRM1 and LCD; we selectively labeled and detected these sites to further probe the outer domains. We were not able to detect these pairs after double CP selection (with an incoming gas to control the sample temperature at 263 K), likely because of residual motions and possibly from peak broadening due to disorder in these domains. The $^{13}C[^{15}N]$ rotational-echo, double-resonance (33) difference spectrum of the AG/AY selectively labeled fl TIA1, however, revealed broad peaks in the coil or sheet region (see *SI Appendix*, Fig. S6) (32). In aggregate these observations support the idea that RRM1 and LCD are dynamic and possibly polymorphic.

To test our hypothesis that RRM2 and RRM3 are folded in fl TIA1, we confirmed whether our NMR spectra agreed adequately well with known structures and spectra of a RRM2,3 construct. We compared the chemical shifts for fl TIA1 to those

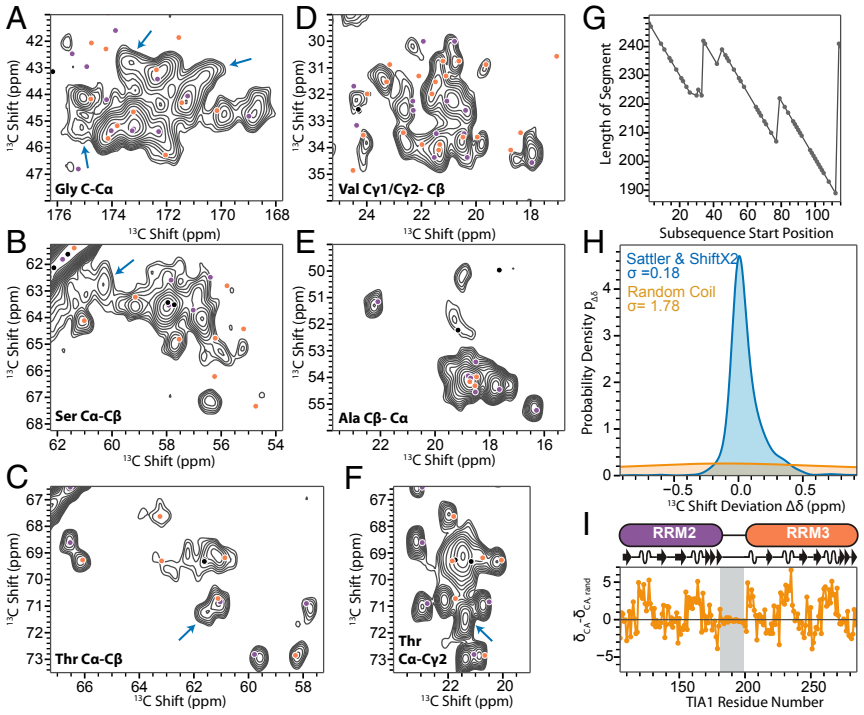

Fig. 2. (*A*–*F*) Solid-state NMR ^{13}C–^{13}C CP MAS spectra of apo fl U–^{13}C,^{15}N TIA1 (spontaneously oligomerized as described in the text) expanded to highlight specific amino acids. Solution-state NMR chemical shift positions of the RRM2,3 excised domains (11) are indicated with circles (purple: RRM2, orange: RRM3, black: loop between RRM2 and RRM3). Generally, the chemical shifts of the fl TIA1 match those of the excised RRM2,3 domains. Blue arrows point to a few experimental peaks that do not agree well with RRM2,3 peaks from excised domains. The mixing time was 20 ms, and the magnetic field was 21.1 T [$\nu_0(^1H)$ = 900 MHz]. Lowest contours are at 3.5× RMS noise, and others are 1.25× higher. (*G*) We identify a contiguous amino acid construct within fl TIA1 that could explain the number of resolved experimental peaks for specific amino acid types in these spectra. The number of residues needed is plotted as a function of the assumed beginning residue number (assuming a single contiguous observable segment). A construct beginning near residue 110 is the minimum construct needed to explain all peaks; if the construct were to begin after residue 130, several peaks would be unexplained. The minimum length segment needed to explain the observed peaks spans RRM2 and RRM3. Comparison of assigned chemical shifts in the ^{13}C–^{13}C DARR spectrum of fl TIA1 with those from two structural models. (*H*) Probability densities of the deviation between measured and predicted chemical shifts using Gaussian kernel density estimation. The chemical shifts from the isolated RRM domains match well shifts observed here for apo fl oligomeric TIA1 (blue). Most observed chemical shifts for apo fl oligomeric TIA1 are not compatible with a random coil (orange). (*I*) The difference between experimental Cα chemical shifts and those predicted for a random coil model (Poulsen's intrinsically disordered protein chemical shifts) is large (rejecting the IDP model) for RRM2 and RRM3 but small for the linker between them, suggesting that this segment is unstructured in the apo fl oligomeric TIA1. The locations of helix and sheet segments are shown schematically.

observed or predicted for the folded globular RRM domains. We compared our results to published solution-state NMR chemical shifts for the human RRM2,3 construct wherever the residues are identical in human and mouse (11, 13). To account for the three mutations that differentiate the mouse sequence used here (*SI Appendix*, Fig. S7) and the human sequence in the RRM2,3 regions used in solution NMR studies, the missing data were predicted. A homology model was constructed using Schrödinger Prime (34), and chemical shifts were predicted from the homology model using ShiftX2 (35), a machine learning–based tool that predicts chemical shifts with rms errors for N, Cα, and Cβ as low as 1.1, 0.44, and 0.52 parts per million (ppm), respectively. The predicted or previously reported shifts for RRM2 and RRM3 align well with the experimental peaks, as shown in Fig. 2 and *SI Appendix*, Fig. S8.

The following assignment procedure was used to compare the predicted and experimental peaks: 1) If there were no experimental peaks close to a predicted peak (within 0.6 ppm for ^{13}C and/or 1.5 ppm for ^{15}N), the predicted peak was considered unobserved and unassigned. Most of the unobserved peaks arose from RRM1 and the LCD, while a few arose from presumably mobile segments such as loops in the solution RRM2,3 structure. 2) The remaining predicted peaks were matched to the experimental peaks as follows: 1) If a predicted peak was within 0.6 ppm for ^{13}C and 1 ppm for ^{15}N of an experimental peak and no other predicted peaks were within this range, the pair was considered to match, and the peak was considered to be assigned. 2) If a predicted peak was near the experimental peak but there were other predicted peaks and/or experimental peaks in the same range, these were considered to be ambiguously matched or ambiguously assigned. In these cases, we looked for other expected correlations elsewhere in 2D or 3D datasets (listed in *Methods*) to provide additional evidence for the assignments. An example of a backbone walk based on NCACX and NCOCX 3D data is shown in Fig. 3. An overview of the residues that were identified in the 3D experiments is shown in *SI Appendix*, Fig. S10. Overall, 113 residues with residue numbers between 105 and 298 had sites classified as unambiguous based on multidimensional correlations and the above scheme, while 67 residues were ambiguously assigned. For the RRM2,3 domains, the rmsd between the predicted shifts and the shifts assigned in the ^{13}C–^{13}C dipolar assisted rotational resonance (DARR) spectra alone was 0.2 ppm, as shown in Fig. 2*H*. This excellent agreement indicates with high confidence that the RRM2 and RRM3 domains have the same fold in fl TIA1 as in globular, isolated domains. We also compared the assigned chemical shifts to random coil shifts, and only the loop segment connecting RRM2 and RRM3 was compatible with an unfolded model (see Fig. 2*I*).

If the C-terminal LCD had formed amyloid-like fibrils, many of the residues in this segment would be expected to be ordered and detectable in CP magic-angle spinning (MAS) experiments. Furthermore, they would be expected to have chemical shifts consistent with β-sheet secondary structure (32). We did not observe these residues or a preponderance of β-sheet amino acids. Thus, we concluded that the NMR signals of the LCD are poorly detected in fl TIA1, presumably because this domain is dynamic on an intermediate timescale (roughly 10 ms to 10 ns) and, in particular, is not an ordered, amyloid-like species. For further comparison, we prepared a TIA1 construct containing only the LCD (TIA1-LCD) analogously to the fl with a cleavable solubility tag. As shown in Fig. 4, the ^{13}C-^{13}C SSNMR spectrum of TIA1-LCD (295 to 387), prepared comparably, has many broad and unresolved peaks, suggesting a high amount of static disorder. Interestingly, there are many peaks in the TIA1-LCD sample not found in fl TIA1 spectra. These data indicate that the excised LCD in our hands does not recapitulate the structure and dynamics of the LCD in fl TIA1. We therefore did not study the TIA1-LCD domain further.

Discussion

Full-length TIA1 is shown to form a dense colloidal-like phase stably and reversibly. The reproducible NMR spectra of fl TIA1 (*SI Appendix*, Fig. S3) exhibit strong CP MAS SSNMR signals from the RRM2 and RRM3 domains, indicating that these functionally critical domains are ordered. By contrast, signals are

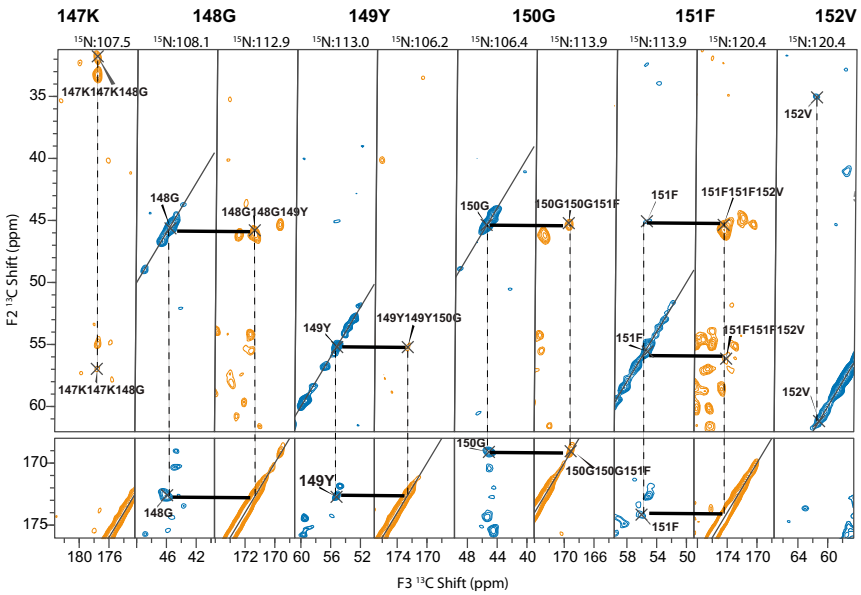

Fig. 3. Example strips from 3D NCACX (blue) and 3D NCOCX (orange) experiments on fl TIA1. The strips show a backbone walk from 147K to 152V. Only the peak labels for these residues are shown for simplicity; the additional labels from this plane are shown in *SI Appendix*, Fig. S9. While there is not enough resolution in the strips to perform a complete de novo assignment, many of the chemical shifts from the liquid-state model are confirmed in the experiment. The NCOCX was collected on a 900 MHz spectrometer. The NCACX was collected on a 750 MHz spectrometer. The contour levels are incremented by a factor of 1.25.

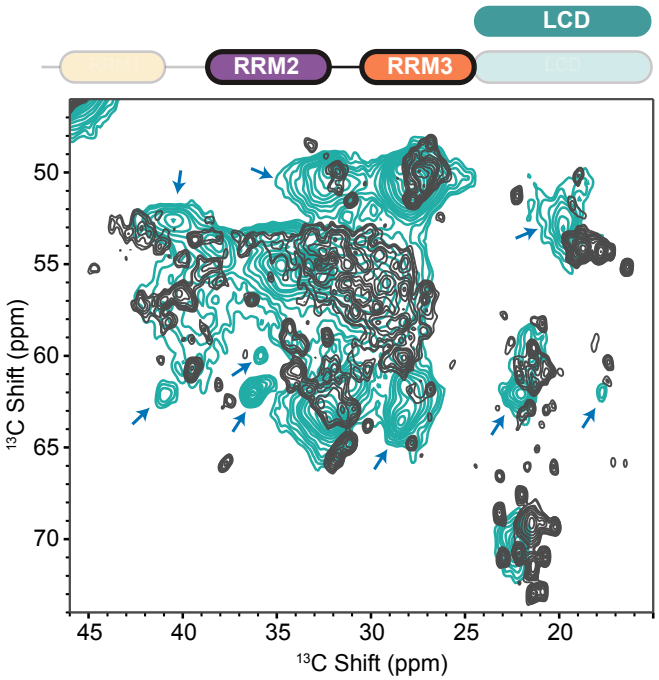

Fig. 4. The ^{13}C-^{13}C CP MAS spectra of TIA1 (black) and the excised TIA1-LCD (295–386) (teal) prepared with similar protocols. TIA1-LCD displays many resonances not observed in the full-length protein; some are marked with blue arrows. These differences indicate that the structure of the LCD/PRD is different in isolation from the full protein.

generally missing for RRM1 and the LCD, indicating dynamic disorder. Notably, these regions were also missing in insensitive nuclei enhancement by polarization transfer-based sequences, suggesting that the disorder is on too slow a timescale to detect the signals by typical solution NMR methods (e.g., longer than low nanosecond), while too fast for typical solid-state NMR methods (e.g., faster than long millisecond timescale). Chemical shifts for RRM2 and RRM3 are similar to those of the previously studied corresponding soluble domains, indicating these domains are folded and likely functional in the fl apo form. Moreover, residues in RRM2 and RRM3 generally exhibit a single narrow NMR peak for each site, consistent with our suggestion that these domains are well ordered. These data suggest that apo fl TIA1 is not necessarily prone to forming amyloids under mild buffer conditions.

It is surprising that the LCD in the fl TIA1 does not present as an amyloid but instead as a highly disordered species, given the prior literature (26, 28). We see no evidence for cross-β or amyloid structures; indeed, NMR signals are mostly absent for the LCD, suggesting a high degree of dynamic disorder. Our result stands in stark contrast to studies of many other analogously structured proteins. Yeast SUP35 (36) and URE2 (37); fungal HET-S (38); and human TDP-43 (39, 40), FUS (29), and RIPK1/RIPK3 (41) all contain functional RRM or kinase domains and an LCD. These systems have been demonstrated to aggregate into amyloids or prions. In most other studies, the other non-amyloid (putatively functional) domains were disordered or undetected. The fact that TIA1 instead forms a reproducible dense colloid-like phase with ordered, functional domains might be related to sequence differences compared to the other systems since fl TIA1 forms liquid–liquid separated droplets under other conditions (42). We may have formed the specific phase described here because of the mild sample conditions selected or the lack of substrate.

Perhaps fl apo TIA1 with folded and functional RRM2 and RRM3 domains, as described in this work, represents a different stage of maturation than the amyloid forms and may serve as a superior model for TIA1 in stress granules. Stress granules are, of course, considerably more complex, in that they contain multiple other proteins and nucleic acids, but nonetheless, the observation of a stable oligomeric apo form is interesting in terms of the process of stress granule formation. In one limiting model, colocalization and condensation of TIA1 might be initiated in cells when RRMs from different monomers initially bind proximally on long RNA stretches. Subsequently, they may associate with RRMs from other TIA1 monomers (43). The LCDs could then stabilize this complex by interacting with other LCDs from different TIA1 monomers. The order of events is not firmly known; it is also possible that the LCDs initiate oligomerization, whereupon the colocalized RRMs have increased avidity for RNA due to multivalence. The existence of the stable colloidal-like homo-oligomeric apo fl TIA1 (in the absence of RNA) with highly ordered and folded RRMs suggests that the latter hypothesis (LCD-initiated, multivalent, high-avidity RRM–RNA binding) is a plausible picture.

How might the well-folded RRM2,3 domains be compatible structurally with the dynamically disordered RRM1 and LCD in the same molecule? We propose that the organization of fl TIA1 may resemble a micellar structure, as illustrated in Fig. 5. Liquid–liquid separation on the nanometer scale would drive the formation of a structure with hydrated (*SI Appendix*, Fig. S11), ordered RRM2,3 domains, separated from condensates of viscous, disordered RRM1 and LCD domains. Our EM images offer support for this, as no fibrils were observed under a range of conditions, while there is evidence for semispherical oligomers with at least 6 to 10 monomers and other irregular nanoscale structures. The NMR data provide evidence of this model through the differences in order and evidence of water accessibility to the RRM domains.

Full-length TIA1 in the form described here, wherein the functionally crucial RRM2,3 domains are folded, provides a model for early stages of stress granule formation. A colloidal or micellar structure is preferable to amyloids as a model for RNA

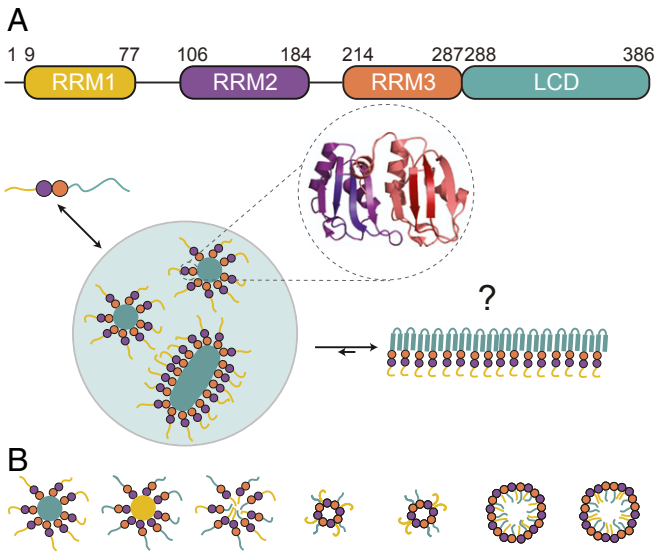

Fig. 5. (*A*) Micellar model for the spatial organization of apo fl oligomeric TIA1 consistent with EM and SSNMR. The RRM2 and RRM3 domains are folded, functional, hydrated, exposed, and ordered. RRM1 and the PRD are disordered and cause nanoscale phase separation but not fibril formation. (*B*) A variety of micellar, oligomeric topologies might be compatible with the available data, illustrated using some limiting cases.

binding and stress granule function because, in vivo, the SG can be formed reversibly and is subject to regulation. Amyloids are typically difficult to disassemble, whereas these dense colloid-like solutions were reversibly formed in our hands. With the stable experimental system and structural model reported here, the stage is set for molecularly detailed follow-on studies of structure, ligand binding, dynamics, and maturation.

Data and Materials Availability. Raw NMR data files, processing, and analysis scripts are available upon request. All study data are included in the article and *SI Appendix*.

ACKNOWLEDGMENTS. The authors thank K. Karl of the Kandel group for stimulating discussions, a plasmid coding for the mouse TIA1 sequence, and TEV protease. K.J.F., J.B.R., E.R.K., and A.E.M. thank Cohen Veteran Bioscience and the US National Science Foundation (Award MCB1412253) for generous support. K.J.F. was supported by a postdoctoral fellowship from NIH (Grant GM128290). The NMR data were collected at the New York Structural Biology Center (NYSBC) with support from the Center on Macromolecular Dynamics by NMR Spectroscopy, a Biomedical Technology Research Resource NIH (Grant GM118302). EM was performed at the Simons EM Center and National Resource for Automated Molecular Microscopy, supported by grants from the Simons Foundation (Grant SF349247) and NIH (Grant GM103310). The NYSBC is also supported by the Empire State Division of Science Technology and Innovation and Office of Research Infrastructure Program (NIH Grant CO6RR015495).

1. Q. Tian, M. Streuli, H. Saito, S. F. Schlossman, P. Anderson, A polyadenylate binding protein localized to the granules of cytolytic lymphocytes induces DNA fragmentation in target cells. *Cell* **67**, 629–639 (1991).
2. A. Kawakami *et al*., Identification and functional characterization of a TIA-1-related nucleolysin. *Proc. Natl. Acad. Sci. U.S.A.* **89**, 8681–8685 (1992).
3. N. Kedersha, P. Anderson, Stress granules: Sites of mRNA triage that regulate mRNA stability and translatability. *Biochem. Soc. Trans.* **30**, 963–969 (2002).
4. M. Piecyk *et al*., TIA-1 is a translational silencer that selectively regulates the expression of TNF-alpha. *EMBO J.* **19**, 4154–4163 (2000).
5. I. López de Silanes *et al*., Identification and functional outcome of mRNAs associated with RNA-binding protein TIA-1. *Mol. Cell. Biol.* **25**, 9520–9531 (2005).
6. P. Anderson, N. Kedersha, RNA granules: Post-transcriptional and epigenetic modulators of gene expression. *Nat. Rev. Mol. Cell Biol.* **10**, 430–436 (2009).
7. S. Kroschwald *et al*., Promiscuous interactions and protein disaggregases determine the material state of stress-inducible RNP granules. *eLife* **4**, e06807 (2015).
8. P. Hackman *et al*., Welander distal myopathy is caused by a mutation in the RNA-binding protein TIA1. *Ann. Neurol.* **73**, 500–509 (2013).
9. J. Klar *et al*., Welander distal myopathy caused by an ancient founder mutation in TIA1 associated with perturbed splicing. *Hum. Mutat.* **34**, 572–577 (2013).
10. I. R. Mackenzie *et al*., TIA1 mutations in amyotrophic lateral sclerosis and frontotemporal dementia promote phase separation and alter stress granule dynamics. *Neuron* **95**, 808–816.e9 (2017).
11. I. Wang *et al*., Structure, dynamics and RNA binding of the multi-domain splicing factor TIA-1. *Nucleic Acids Res.* **42**, 5949–5966 (2014).
12. L. Freiburger *et al*., Efficient segmental isotope labeling of multi-domain proteins using sortase A. *J. Biomol. NMR* **63**, 1–8 (2015).
13. M. Sonntag *et al*., Segmental, domain-selective perdeuteration and small-angle neutron scattering for structural analysis of multi-domain proteins. *Angew. Chem. Int. Ed. Engl.* **56**, 9322–9325 (2017).
14. A. Molliex *et al*., Phase separation by low complexity domains promotes stress granule assembly and drives pathological fibrillization. *Cell* **163**, 123–133 (2015).
15. S. F. Banani, H. O. Lee, A. A. Hyman, M. K. Rosen, Biomolecular condensates: Organizers of cellular biochemistry. *Nat. Rev. Mol. Cell Biol.* **18**, 285–298 (2017).
16. R. Halfmann, A glass menagerie of low complexity sequences. *Curr. Opin. Struct. Biol.* **38**, 18–25 (2016).
17. A. C. Murthy *et al*., Molecular interactions underlying liquid-liquid phase separation of the FUS low-complexity domain. *Nat. Struct. Mol. Biol.* **26**, 637–648 (2019).
18. B. E. Ackermann, G. T. Debelouchina, Heterochromatin protein HP1α gelation dynamics revealed by solid-state NMR spectroscopy. *Angew. Chem. Int. Ed. Engl.* **58**, 6300–6305 (2019).
19. Y. Lin, D. S. Protter, M. K. Rosen, R. Parker, formation and maturation of phase-separated liquid droplets by RNA-binding proteins. *Mol. Cell* **60**, 208–219 (2015).
20. S. Jain *et al*., ATPase-modulated stress granules contain a diverse proteome and substructure. *Cell* **164**, 487–498 (2016).
21. J. R. Buchan, R. M. Kolaitis, J. P. Taylor, R. Parker, Eukaryotic stress granules are cleared by autophagy and Cdc48/VCP function. *Cell* **153**, 1461–1474 (2013).
22. A. F. Harrison, J. Shorter, RNA-binding proteins with prion-like domains in health and disease. *Biochem. J.* **474**, 1417–1438 (2017).
23. B. Wolozin, Regulated protein aggregation: Stress granules and neurodegeneration. *Mol. Neurodegener.* **7**, 56 (2012).
24. D. S. Kryndushkin, I. M. Alexandrov, M. D. Ter-Avanesyan, V. V. Kushnirov, Yeast [PSI+] prion aggregates are formed by small Sup35 polymers fragmented by Hsp104. *J. Biol. Chem.* **278**, 49636–49643 (2003).
25. R. Nelson *et al*., Structure of the cross-beta spine of amyloid-like fibrils. *Nature* **435**, 773–778 (2005).
26. Y. Furukawa, K. Kaneko, G. Matsumoto, M. Kurosawa, N. Nukina, Cross-seeding fibrillation of Q/N-rich proteins offers new pathomechanism of polyglutamine diseases. *J. Neurosci.* **29**, 5153–5162 (2009).
27. X. Li, J. B. Rayman, E. R. Kandel, I. L. Derkatch, Functional role of Tia1/pub1 and Sup35 prion domains: Directing protein synthesis machinery to the tubulin cytoskeleton. *Mol. Cell* **55**, 305–318 (2014).
28. M. Kato *et al*., Cell-free formation of RNA granules: Low complexity sequence domains form dynamic fibers within hydrogels. *Cell* **149**, 753–767 (2012).
29. D. T. Murray *et al*., Structure of FUS protein fibrils and its relevance to self-assembly and phase separation of low-complexity domains. *Cell* **171**, 615–627.e16 (2017).
30. A. C. Murthy, N. L. Fawzi, The (un)structural biology of biomolecular liquid-liquid phase separation using NMR spectroscopy. *J. Biol. Chem.* **295**, 2375–2384 (2020).
31. J. D. Forman-Kay, T. Mittag, From sequence and forces to structure, function, and evolution of intrinsically disordered proteins. *Structure* **21**, 1492–1499 (2013).
32. K. J. Fritzsching, M. Hong, K. Schmidt-Rohr, Conformationally selective multidimensional chemical shift ranges in proteins from a PACSY database purged using intrinsic quality criteria. *J. Biomol. NMR* **64**, 115–130 (2016).
33. T. Gullion, J. Schaefer, Rotational-echo double-resonance NMR. *J. Magn. Reson.* **81**, 196–200 (1989).
34. M. P. Jacobson *et al*., A hierarchical approach to all-atom protein loop prediction. *Proteins* **55**, 351–367 (2004).
35. B. Han, Y. Liu, S. W. Ginzinger, D. S. Wishart, SHIFTX2: Significantly improved protein chemical shift prediction. *J. Biomol. NMR* **50**, 43–57 (2011).
36. A. K. Schütz *et al*., Solid-state NMR sequential assignments of the amyloid core of full-length Sup35p. *Biomol. NMR Assign.* **8**, 349–356 (2014).
37. B. Habenstein *et al*., Extensive de novo solid-state NMR assignments of the 33 kDa C-terminal domain of the Ure2 prion. *J. Biomol. NMR* **51**, 235–243 (2011).
38. C. Wasmer *et al*., Amyloid fibrils of the HET-s(218-289) prion form a beta solenoid with a triangular hydrophobic core. *Science* **319**, 1523–1526 (2008).
39. E. L. Guenther *et al*., Atomic structures of TDP-43 LCD segments and insights into reversible or pathogenic aggregation. *Nat. Struct. Mol. Biol.* **25**, 463–471 (2018).
40. J. Shenoy *et al*., Structural dissection of amyloid aggregates of TDP-43 and its C-terminal fragments TDP-35 and TDP-16. *FEBS J.* **287**, 2449–2467 (2019).
41. M. Mompean *et al*., The structure of the necrosome RIPK1-RIPK3 core, a human hetero-amyloid signaling complex. *Cell* **173**, 1244–1253.e10 (2018).
42. J. B. Rayman, K. A. Karl, E. R. Kandel, TIA-1 self-multimerization, phase separation, and recruitment into stress granules are dynamically regulated by Zn^2. *Cell Rep.* **22**, 59–71 (2018).
43. J. R. Wheeler, T. Matheny, S. Jain, R. Abrisch, R. Parker, Distinct stages in stress granule assembly and disassembly. *eLife* **5**, e18413. (2016).